การวิเคราะห์การสั่นไหวอิสระของคานประกอบโดยวิธีการวิเคราะห์เรขาคณิตเท่าเทียม
Free vibration analysis of composite beams by IGA

พีรภัทร์ น้อยดี[1] และ ศ. ดร.จรูญ รุ่งอมรรัตน์[2]

[1,2] ภาควิชาวิศวกรรมโยธา คณะวิศวกรรมศาสตร์ จุฬาลงกรณ์มหาวิทยาลัย จ.กรุงเทพฯ

Abstract

This senior project investigates free vibration and develops a tool for calculating fundamental frequencies of functionally graded nanocomposite metal foam beams with GPLs dispersed. Both pores and GPLs distributions are varying in thickness direction. The fundamental frequency is calculated using Isogeometric analysis based on Timoshenko beam theory with axial deformation considered and the Hamilton's principle by finding the least eigenvalue from the equation system. The results show approximate answer of dimensionless fundamental frequency compared with results done by using the Ritz method.

Keywords: Isogeometric analysis, Functionally graded metal foam, Nanocomposite beam, Graphene platelet, Timoshenko beam theory

1. Introduction

Steel structures were originally lighter than reinforced concrete structures, while several institutions are studying porous metal or metal foam for the use in lightweight structures, which has high energy absorption and high stiffness-to-weight [1],[2].

Most studies on metal foam currently look at uniform or random distribution of porosity, but new studies developed manufacturing processes that enable to produce functionally graded (FG) porous metal foam, which can allow us to more varietally and freely determine its properties [3],[4][5][6].

Many have used a variety of theories and methods to predict the properties of functionally graded (FG) porous beams, particularly the free vibration which is required for structural applications.

Shafiei et al. [7] investigated size dependent nonlinear vibration on imperfect uniform and non-uniform functionally graded (FG) microbeams. The govern equation is obtained using modified couple stress, Euler–Bernoulli theories, the Von-Kármán's nonlinear strain, Hamilton's principle and Numerical results are obtained using generalized differential quadrature method (GDQM) and direct iterative method.

Chen et al. [8] investigated the free and forced vibration characteristics of functionally graded (FG) porous beams made of open-cell metal foam. The governing equation is obtained using Timoshenko beam theory, Lagrange equation method and results are obtained using Ritz trial functions. They [9] also investigated nonlinear free vibration behavior of sandwich porous beam composed of two face layers and a functionally graded porous core. The governing equation system is derived from Timoshenko beam theory, The Ritz method and von Kármán type nonlinear strain-displacement relationships and solve the governing equation system using direct iterative algorithm.

Reinforcing porous metal with nanofillers can also allow us to more varietally and freely determine its properties and maintain lightweight. Carbonaceous nanofillers such as carbon nanotubes (CNTs) and graphene platelets (GPLs) are of interest, but the experiment showed that GPLs can provide better

enhancement in various of mechanical properties than CNTs [10].

Kitipornchai et al. [11] investigated free vibration and elastic buckling of functionally graded porous nanocomposite metal foam beams where pores and GPLs are uniformly distributed in each layer of multilayer beam model which applied to achieve desired functionally graded properties. The mechanical properties of closed-cell cellular solids under Gaussian Random Field scheme are used to determine the variation of Poisson's ratio and the relationship between porosity coefficients and mass density. The elastic modulus of the nanocomposite is obtained by using Halpin-Tsai micromechanics model. The governing equation is obtained using Timoshenko beam theory with axial deformation considered, the minimum potential energy principle and results are obtained using the Ritz method with polynomial basis function.

The objective of this project is to investigate the free vibration and develop a tool for calculating fundamental frequency of functionally graded porous metal foam beam with one uniform and two non-uniform distributions in both pores and GPLs dispersed varying in the thickness direction by using Timoshenko beam theory with axial deformation considered and the Hamilton's principle by finding the least eigenvalue from the equation system. This research is done in the same way as work done by Kitipornchai et al. but using Isogeometric analysis with B-splines basis function which is piecewisely defined and has the potential to solve the problem of more difficult shaped beams. which allows us to solve more complex beam problems.

2. Porosity distribution and GPL patterns

Consider beam placed on the x, z coordinate system with thickness h along with $x-$axis, width b and length L along with $z-$axis. Three different porosity distributions (1, 2, Uniform) with three different GPL dispersion patterns (A, B, C) were considered. The GPL volume content V_{GPL} is varying along the $z-$axis, as shown in Fig. 1.

where E_1' and E_2' are the maximum and minimum Young's modulus of the beams without GPLs with non-uniform porosity distribution 1, 2 and E' is Young's modulus of beams without GPLs with uniform porosity distribution. s_{ij} $(i, j = 1,2,3)$ are peak values of V_{GPL} for porosity distribution i and GPL dispersion pattern j, which have to be different for different dispersion patterns or porosity distribution to control the total quantity of GPL which must be equal in the comparison between different GPL dispersion patterns or porosity distributions to make the comparison fair.

The Young's modulus, shear modulus and mass density of porous nanocomposite beams with porosity distribution 1, 2 and uniform porosity distribution are defined as follow

$$\begin{cases} E(z) = E_1\left[1-e_0\lambda(z)\right] \\ G(z) = \dfrac{E(z)}{2\left[1+\nu(z)\right]} \\ \rho(z) = \rho_1\left[1-e_m\lambda(z)\right] \end{cases} \tag{1}$$

where

$$\lambda(z) = \begin{cases} \cos\left(\pi z/h\right) & \textit{Porosity distribution 1} \\ \cos\left(\pi z/2h+\pi/4\right) & \textit{Porosity distribution 2} \\ \lambda & \textit{Uniform distribution} \end{cases} \tag{2}$$

where E_1 and ρ_1 are the maximum values of Young's modulus and mass density of the porous nanocomposite respectively and porosity coefficient e_0 is defined as follow

$$e_0 = 1-\frac{E_2'}{E_1'} \tag{3}$$

The mechanical property of closed-cell cellular solids under Gaussian Random Field (GRF) scheme can be expressed as [12]

$$\frac{E(z)}{E_1} = \left(\frac{\rho(z)/\rho_1+0.121}{1.121}\right)^{2.3} \quad 0.15 < \frac{\rho(z)}{\rho_1} < 1 \tag{4}$$

which is used to determine the coefficient of mass density e_m as

$$e_m = \frac{1.121\left(1-\sqrt[2.3]{1-e_0\lambda(z)}\right)}{\lambda(z)} \tag{5}$$

and was also used to determine Poisson's ratio $\nu(z)$ as follow [13]

$$\nu(z) = 0.221p' + \nu_1\left(0.342p'^2 - 1.21p' + 1\right) \tag{6}$$

where ν_1 is Poisson's ratio of pure matrix materials without pores and

$$p' = 1-\frac{\rho(z)}{\rho_1} = 1.121\left(1-\sqrt[2.3]{1-e_0\lambda(z)}\right) \tag{7}$$

In the comparison, the total masses of the beams must be controlled for different porosity distributions. Then λ in Eq. (2) can be derived as

$$\lambda = \frac{1}{e_0} - \frac{1}{e_0}\left(\frac{M/\rho_1 h+0.121}{1.121}\right)^{2.3} \tag{8}$$

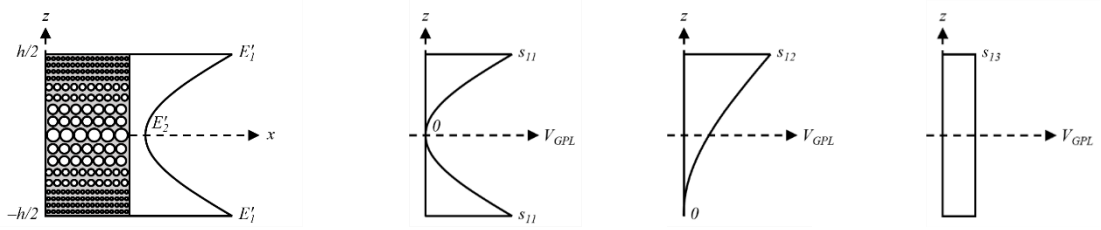

(A) Non-uniform porosity distribution 1 with three GPL dispersion patterns

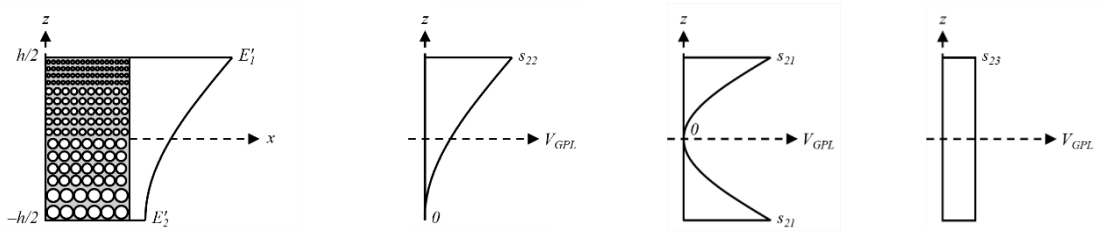

(B) Non-uniform porosity distribution 2 with three GPL dispersion patterns

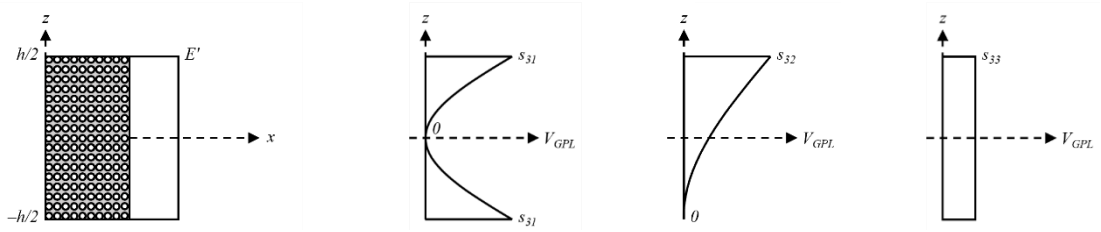

(C) Uniform porosity distribution with three GPL dispersion patterns

Fig. 1. Porosity distributions and GPL dispersion patterns.

where M is equal for all three porosity distributions and can be calculated by

$$M = \int_{-h/2}^{h/2} \rho_1 \left(1 - p'\right) dx \tag{9}$$

According to GPL dispersion pattern as shown in Fig. 1. Volume fraction of GPLs V_{GPL} for those patterns are $(i = 1,2,3)$

$$V_{GPL} = \begin{cases} s_{i1}\left[1 - \cos\left(\pi z/h\right)\right] & Pattern\,A \\ s_{i2}\left[1 - \cos\left(\pi z/2h + \pi/4\right)\right] & Pattern\,B \\ s_{i3} & Pattern\,C \end{cases} \tag{10}$$

weight fraction Λ_{GPL} of GPL nanofillers is related volume fraction as follow

$$\frac{\Lambda_{GPL}}{\Lambda_{GPL} + \frac{\rho_{GPL}}{\rho_M} - \frac{\rho_{GPL}}{\rho_M}\Lambda_{GPL}} \times \int_{-h/2}^{h/2} \left[1 - e_m \lambda(z)\right] dz = \int_{-h/2}^{h/2} V_{GPL}\left[1 - e_m \lambda(z)\right] dz \tag{11}$$

The Halpin-Tsai micromechanics model [10],[14],[15],[16] is used to determine elastic modulus of nanocomposites without pores. It is assumed that the non-porous GPL-reinforced metal matrix is randomly oriented short fiber reinforced composite. Then

$$E_1 = \frac{3}{8}\left(\frac{1 + \xi_L^{GPL}\eta_L^{GPL}V_{GPL}}{1 - \eta_L^{GPL}V_{GPL}}\right)E_M + \frac{5}{8}\left(\frac{1 + \xi_W^{GPL}\eta_W^{GPL}V_{GPL}}{1 - \eta_W^{GPL}V_{GPL}}\right)E_M \tag{12}$$

which

$$\xi_W^{GPL} = \frac{2l_{GPL}}{t_{GPL}} \tag{13}$$

$$\xi_W^{GPL} = \frac{2w_{GPL}}{t_{GPL}} \tag{14}$$

$$\eta_L^{GPL} = \frac{\left(E_{GPL}/E_M\right) - 1}{\left(E_{GPL}/E_M\right) + \xi_L^{GPL}} \tag{15}$$

$$\eta_W^{GPL} = \frac{\left(E_{GPL}/E_M\right) - 1}{\left(E_{GPL}/E_M\right) + \xi_W^{GPL}} \tag{16}$$

where w_{GPL}, l_{GPL} and t_{GPL} are average width, length and thickness of GPLs and E_M คือ Young's modulus of metal matrix.

Mass density ρ_1 and Poisson's ratio ν_1 of GPL-reinforced metal matrix can be calculated from rule of mixture as follow

$$\rho_1 = \rho_{GPL} V_{GPL} + \rho_M V_M \tag{17}$$

$$\nu_1 = \nu_{GPL} V_{GPL} + \nu_M V_M \tag{18}$$

which $\rho_1, \nu_1, V_{GPL}, \rho_M, \nu_M$ and V_M are mass density, Poisson's ratio and GPLs' volume fraction and metal matrix respectively and $V_M = 1 - V_{GPL}$ (19)

3. Formulations

3.1 Lagrangian for the proposed beam

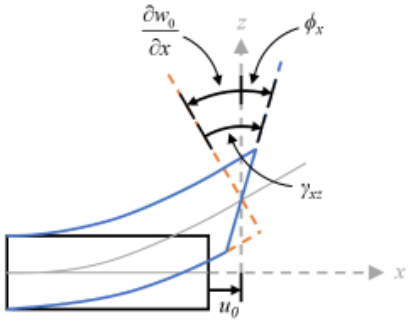

Fig. 2. Rotation in Timoshenko beam theory with axial deformation considered.

The beam theory used in this project is Timoshenko beam theory with axial deformation considered. So, beam's displacement component in the $x-$ and $z-$directions are

$$\begin{cases} u_x(x,z,t) = u_0(x,t) + z\phi_x(x,t) \\ w_z(x,z,t) = w_0(x,t) \end{cases} \tag{20}$$

where $u_0(x,t)$, $w_0(x,t)$ are axial displacement, transverse displacement at mid-plane $(z=0)$, $\phi_x(x,t)$ is transverse normal rotation about $z-$axis and t is time.

As shown in Fig. 2, axial and transverse shear strain are as follow

$$\begin{cases} \varepsilon_{xx} = \dfrac{\partial u_0}{\partial x} + z\dfrac{\partial \phi_x}{\partial x} \\ \gamma_{xz} = \dfrac{\partial w_0}{\partial x} + \phi_x \end{cases} \tag{21}$$

Under the linear stress-strain constitutive law, Normal and transverse stress are in forms of

$$\begin{cases} Q_{xx} = Q_{11}(z)\varepsilon_{xx} \\ Q_{xz} = Q_{55}(z)\gamma_{xz} \end{cases} \tag{22}$$

where

$$\begin{cases} Q_{11}(z) = \dfrac{E(z)}{1-\nu^2(z)} \\ Q_{55}(z) = G(z) \end{cases} \tag{23}$$

Variation of strain energy δU can be written as

$$\delta U = \int_0^L \Big[A_{11}u_0'\delta u_0' + B_{11}\left(u_0'\delta\phi_x' + \phi_x'\delta u_0'\right) + D_{11}\phi_x'\delta\phi_x' + A_{55}\left(w_0'\delta w_0' + w_0'\delta\phi_x + \phi_x\delta w_0' + \phi_x\delta\phi_x\right)\Big]dx \tag{24}$$

where the stiffness quantities are

$$\begin{cases} \{A_{11}, B_{11}, D_{11}\} = \displaystyle\int_{-h/2}^{h/2} Q_{11}(z)\{1, z, z^2\}dz, \\ A_{55} = \displaystyle\int_{-h/2}^{h/2} kQ_{55}(z)dz \end{cases} \tag{25}$$

which $k = 5/6$ is shear correction factor of considered beam's section

Variation of kinetic energy δT and variation of external work δW_E due to external axial load N_{x0} can be written as

$$\delta T = \int_0^L \Big[I_0\dot{u}_0\delta\dot{u}_0 + I_1\left(\dot{u}_0\delta\dot{\phi}_x + \dot{\phi}_x\delta\dot{u}_0\right) + I_2\dot{\phi}_x\delta\dot{\phi}_x + I_0\dot{w}_0\delta\dot{w}_0\Big]dx \tag{26}$$

$$\delta W_E = \int_0^L \Big[N_{x0}w_0'\delta w_0' \Big]dx \tag{27}$$

where the inertia quantities are

$$\{I_0, I_1, I_{12}\} = \int_{-h/2}^{h/2} \rho(z)\{1, z, z^2\}dz \tag{28}$$

Define these quantities in dimensionless form as follows

$$\begin{aligned} &\{u, w\} = \frac{\{u_0, w_0\}}{h}, \phi = \phi_x, \xi = \frac{x}{L}, \\ &\eta = \frac{L}{h}, \tau = t\sqrt{\frac{A^*}{I^*L^2}}, \omega = \Omega L\sqrt{\frac{A^*}{I^*}}, \\ &\{a_{11}, b_{11}, d_{11}, a_{55}\} = \left\{\frac{A_{11}}{A^*}, \frac{B_{11}}{A^*h}, \frac{D_{11}}{A^*h^2}, \frac{A_{55}}{A^*}\right\}, \\ &\{t_0, t_1, t_2\} = \left\{\frac{I_0}{I^*}, \frac{I_1}{I^*h}, \frac{I_2}{I^*h^2}\right\} \end{aligned} \tag{29}$$

where A^* and I^* are the values of A_{11} and I_0 of pure metal beam without pores and nanofillers and ω is the dimensionless natural frequency Ω

the Hamilton's principle

$$\int_{t_1}^{t_2} \delta T - \delta U + \delta W_E = 0 \quad \forall(t_1, t_2) \tag{30}$$

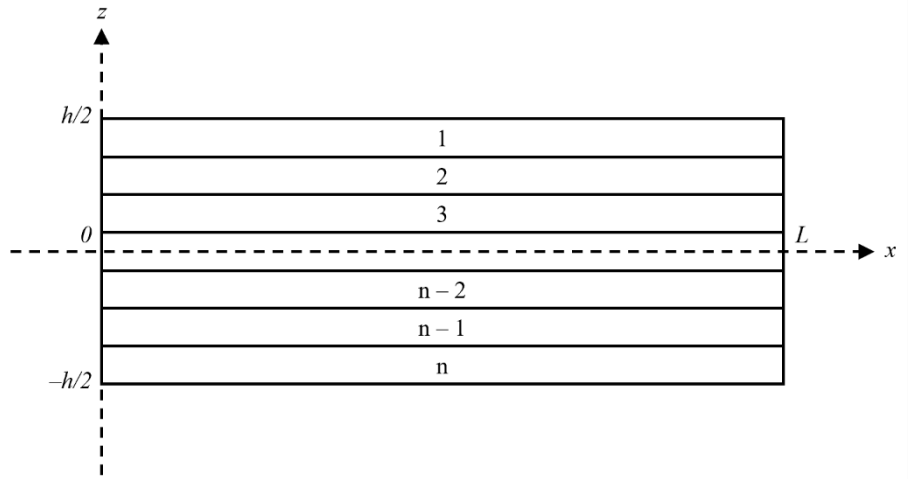

Fig. 3. A multilayer beam model.

Let $u(\xi,\tau), w(\xi,\tau), \phi(\xi,\tau)$ are periodic functions as follows:

$$\begin{aligned}&\{u(\xi,\tau), w(\xi,\tau), \phi(\xi,\tau)\}\\&\quad=\{u^*(\xi), w^*(\xi), \phi^*(\xi)\}e^{i\omega\tau}\end{aligned} \tag{31}$$

where $i=\sqrt{-1}$

Substituting Eq. (24), (26), (27), (29) and (31) into Eq. (30) and set $N_{x0} = 0$ because of consider free vibration gives

$$\begin{aligned}&\left\{\int_0^1 [L_1+L_2+L_3]d\xi\right\}+\eta\left\{\int_0^1 [L_4+L_5]d\xi\right\}\\&\quad+\eta^2\left\{\int_0^1 [L_6]d\xi\right\}-\omega^2\left\{\int_0^1 [L_7+L_8+L_9]d\xi\right\}=0\\&\qquad\qquad\forall\delta u^*,\delta w^*,\delta\phi^*\end{aligned} \tag{32}$$

where

$$\begin{aligned}L_1&=\frac{d\delta u^*(\xi)}{d\xi}\left(a_{11}\frac{du^*(\xi)}{d\xi}+b_{11}\frac{d\phi^*(\xi)}{d\xi}\right)\\L_2&=\frac{d\delta\phi^*(\xi)}{d\xi}\left(b_{11}\frac{du^*(\xi)}{d\xi}+d_{11}\frac{d\phi^*(\xi)}{d\xi}\right)\\L_3&=\frac{d\delta w^*(\xi)}{d\xi}a_{55}\frac{dw^*(\xi)}{d\xi}\\L_4&=\delta\phi^*(\xi)a_{55}\frac{dw^*(\xi)}{d\xi}\\L_5&=\frac{d\delta w^*(\xi)}{d\xi}a_{55}\phi^*(\xi)\\L_6&=\delta\phi^*(\xi)a_{55}\phi^*(\xi)\\L_7&=\delta u^*(\xi)\left(\iota_0 u^*(\xi)+\iota_1\phi^*(\xi)\right)\\L_8&=\delta\phi^*(\xi)\left(\iota_1 u^*(\xi)+\iota_2\phi^*(\xi)\right)\\L_9&=\delta w^*(\xi)\iota_0 w^*(\xi)\end{aligned} \tag{33}$$

For ease of manufacturing, a multilayer beam model made up of n layers of the same thickness ($\Delta h = h/n$) as shown in Fig. 3 is used to achieve the desired porosity distribution and GPL volume content. Where porosity and quantity of GPL are constant within each individual layer by using values at the layer's mid-plane.

So, the dimensionless stiffness and inertia quantities can be calculated as follow

$$a_{11}=\frac{1-\nu_M^2}{nE_M}\sum_{i=1}^{n}\frac{E_1(h\alpha)\left[1-e_0\lambda(h\alpha)\right]}{1-\nu^2(h\alpha)} \tag{34}$$

$$b_{11}=\frac{1-\nu_M^2}{nE_M}\sum_{i=1}^{n}\frac{E_1(h\alpha)\left[1-e_0\lambda(h\alpha)\right]}{1-\nu^2(h\alpha)}(\alpha) \tag{35}$$

$$d_{11}=\frac{1-\nu_M^2}{nE_M}\sum_{i=1}^{n}\frac{E_1(h\alpha)\left[1-e_0\lambda(h\alpha)\right]}{1-\nu^2(h\alpha)}(\alpha)^2 \tag{36}$$

$$a_{55}=\frac{1-\nu_M^2}{nE_M}\sum_{i=1}^{n}k\frac{E_1(h\alpha)\left[1-e_0\lambda(h\alpha)\right]}{2\left[1+\nu(h\alpha)\right]} \tag{37}$$

$$\iota_0=\frac{1}{n\rho_M}\sum_{i=1}^{n}\rho_1(h\alpha)\left[1-e_m\lambda(h\alpha)\right] \tag{38}$$

$$\iota_1=\frac{1}{n\rho_M}\sum_{i=1}^{n}\rho_1(h\alpha)\left[1-e_m\lambda(h\alpha)\right](\alpha) \tag{39}$$

$$\iota_2=\frac{1}{n\rho_M}\sum_{i=1}^{n}\rho_1(h\alpha)\left[1-e_m\lambda(h\alpha)\right](\alpha)^2 \tag{40}$$

where

$$\alpha=\frac{1}{2}+\frac{1}{2n}-\frac{i}{n}\quad\left(i=1,2,3,...,n\right) \tag{41}$$

3.2 Free vibration analysis

The analysis of free vibration is performed using Isogeometric Analysis method. B-splines basis functions is used to approximate the trial function u^*, w^*, ϕ^* and test

function $\delta u^*, \delta w^*, \delta\phi^*$ which is piecewisely defined on ξ as follows

$$N_{i,0}(\xi) = \begin{cases} 1 & if\ \xi_i \le \xi < \xi_{i+1}, \\ 0 & otherwise. \end{cases} \tag{42}$$

$$N_{i,p}(\xi) = \frac{\xi - \xi_i}{\xi_{i+p} - \xi_i} N_{i,p-1}(\xi) + \frac{\xi_{i+p+1} - \xi}{\xi_{i+p+1} - \xi_{i+1}} N_{i+1,p-1}(\xi) \tag{43}$$

where i is index of basis function, p is polynomial order of basis function, n is the number of basis functions used to construct the B-spline curve and ξ_j is the j^{th} knot of knot vector $\Xi = \{\xi_1, \xi_2, \xi_3, \ldots, \xi_{n+p-1}, \xi_{n+p}, \xi_{n+p+1}\}$

The knot vector to use in this problem is an open, uniform knot vector, where ξ_j has the following values

$$\xi_j = \begin{cases} 0 & j \in [1, p+1] \\ \dfrac{j-p-1}{n-p} & j \in [p+2, n] \\ 1 & j \in [n+1, n+p+1] \end{cases} \tag{44}$$

So, the trial functions are as follows

$$\begin{Bmatrix} u^*(\xi) \\ w^*(\xi) \\ \phi^*(\xi) \end{Bmatrix} = \boldsymbol{N} \times \begin{Bmatrix} \boldsymbol{\alpha}_u \\ \boldsymbol{\alpha}_w \\ \boldsymbol{\alpha}_\phi \end{Bmatrix}, \quad \begin{Bmatrix} (u^*)'(\xi) \\ (w^*)'(\xi) \\ (\phi^*)'(\xi) \end{Bmatrix} = \boldsymbol{N}' \times \begin{Bmatrix} \boldsymbol{\alpha}_u \\ \boldsymbol{\alpha}_w \\ \boldsymbol{\alpha}_\phi \end{Bmatrix} \tag{45}$$

and test functions are as follows

$$\begin{Bmatrix} \delta u^*(\xi) \\ \delta w^*(\xi) \\ \delta\phi^*(\xi) \end{Bmatrix} = \begin{Bmatrix} \boldsymbol{\beta}_u^T \\ \boldsymbol{\beta}_w^T \\ \boldsymbol{\beta}_\phi^T \end{Bmatrix} \times \boldsymbol{N}^T, \quad \begin{Bmatrix} \delta(u^*)'(\xi) \\ \delta(w^*)'(\xi) \\ \delta(\phi^*)'(\xi) \end{Bmatrix} = \begin{Bmatrix} \boldsymbol{\beta}_u^T \\ \boldsymbol{\beta}_w^T \\ \boldsymbol{\beta}_\phi^T \end{Bmatrix} \times (\boldsymbol{N}')^T \tag{46}$$

where $\boldsymbol{\alpha_u}$, $\boldsymbol{\alpha_w}$, $\boldsymbol{\alpha_\phi}$, $\boldsymbol{\beta_u}$, $\boldsymbol{\beta_w}$, $\boldsymbol{\beta_\phi}$ are $n \times 1$ coefficient column vector as follows

$$\boldsymbol{\alpha}_u = \begin{Bmatrix} \alpha_{u1} \\ \vdots \\ \alpha_{un} \end{Bmatrix}, \quad \boldsymbol{\alpha}_w = \begin{Bmatrix} \alpha_{w1} \\ \vdots \\ \alpha_{wn} \end{Bmatrix}, \quad \boldsymbol{\alpha}_\phi = \begin{Bmatrix} \alpha_{\phi 1} \\ \vdots \\ \alpha_{\phi n} \end{Bmatrix},$$

$$\boldsymbol{\beta}_u = \begin{Bmatrix} \beta_{u1} \\ \vdots \\ \beta_{un} \end{Bmatrix}, \quad \boldsymbol{\beta}_w = \begin{Bmatrix} \beta_{w1} \\ \vdots \\ \beta_{wn} \end{Bmatrix}, \quad \boldsymbol{\beta}_u = \begin{Bmatrix} \beta_{\phi 1} \\ \vdots \\ \beta_{\phi n} \end{Bmatrix} \tag{47}$$

and

$$\boldsymbol{N} = \begin{Bmatrix} N_{1,p}(\xi) & \ldots & N_{n,p}(\xi) \end{Bmatrix} \tag{48}$$

$$\boldsymbol{N}' = \begin{Bmatrix} \dfrac{d}{d\xi} N_{1,p}(\xi) & \ldots & \dfrac{d}{d\xi} N_{n,p}(\xi) \end{Bmatrix} \tag{49}$$

Substituting Eqs. (45) and (46) into Eq. (32) gives final governing equation for analyzing free vibration in the form of

$$\left(\boldsymbol{K} - \omega^2 \boldsymbol{M}\right)\boldsymbol{\alpha} = \boldsymbol{0} \tag{50}$$

where $\boldsymbol{K}$, $\boldsymbol{M}$ are $3n \times 3n$ stiffness matrix, mass matrix and $\boldsymbol{\alpha}$, $\boldsymbol{0}$ are $3n \times 1$ unknown coefficient column vector, zero column vector

In this project, 3 types of support beams will be considered as follows: hinged–hinged (H–H), clamped–clamped (C–C), and clamped–free (C–F). Due to the properties of the open knot vector B-splines basis function, the treatment of essential boundary conditions can be achieved by set these α equal to zero as follows:

Table 1 Treatment of essential boundary conditions for each support types

Support types	α_{u1}	α_{un}	α_{w1}	α_{wn}	$\alpha_{\phi 1}$	$\alpha_{\phi n}$
H–H	0	0	0	0	–	–
C–C	0	0	0	0	0	0
C–F	0	–	0	–	0	–

This can be done by partitioning the matrix system Eq. (55) and other coefficient still the unknown of the system.

Then solve the eigenvalue problem from the partitioned matrix system. The lowest eigenvalue is the dimensionless fundamental frequency.

4. Numerical results

This section shows the numerical results of the described procedure. First result validation which was done by comparing with the approximate solutions done by Kitipornchai et al. [11] which were done by using the Ritz method and author's solutions were done by using $p = 3$, $n = 25$ B-splines. Finally, the convergence studies with various order and number of B-splines basis functions.

where properties of the matrix material are as shown in Table 2

Table 2 Properties of matrix materials.

	Young's modulus (GPa), E_M	Density (kg/m^3), ρ_M	Poisson's ratio, ν_M
Aluminium	68.3	2689.8	0.34
Magnesium	45	1740	0.35
Copper	130	8960	0.34
Nickel	210	8908	0.31
Titanium	116	4506	0.33

and material properties and geometry parameters of GPLs are $w_{GPL} = 1.5\ \mu m$, $l_{GPL} = 2.5\ \mu m$, $t_{GPL} = 1.5\ nm$, $E_{GPL} = 1.01\ TPa$, $\rho_{GPL} = 1062.5\ kg/m^3$, $v_{GPL} = 0.186$ [10],[17]

4.1 Result validation

4.1.1 Effect of varying porosity coefficients e_0 and number of layers n on dimensionless fundamental frequency (porosity distribution 1, GPL pattern A, C–C copper-matrix beam, $L/h = 20$) is shown in Table 3.

Table 3 Result comparison on effect of varying e_0 and n

Λ_{GPL}	n	$e_0 = 0$	$e_0 = 0.2$	$e_0 = 0.4$	$e_0 = 0.6$
Author's solution (ω)					
1 wt.%	2	0.3376	0.3217	0.3042	0.2844
1 wt.%	6	0.4390	0.4336	0.4289	0.4258
1 wt.%	10	0.4464	0.4421	0.4388	0.4372
1 wt.%	14	0.4484	0.4444	0.4414	0.4403
1 wt.%	18	0.4492	0.4454	0.4425	0.4415
1 wt.%	10000	0.4505	0.4468	0.4442	0.4435
0 wt.%	14	0.3159	0.3134	0.3121	0.3128
0 wt.%	10000	0.3167	0.3144	0.3132	0.3142
Solutions done by Kitipornchai et al. (ω)					
1 wt.%	2	0.3376	0.3217	0.3042	0.2845
1 wt.%	6	0.4390	0.4336	0.4289	0.4259
1 wt.%	10	0.4464	0.4421	0.4388	0.4372
1 wt.%	14	0.4484	0.4444	0.4415	0.4403
1 wt.%	18	0.4492	0.4454	0.4426	0.4416
1 wt.%	10000	0.4505	0.4468	0.4442	0.4436
0 wt.%	14	0.3159	0.3134	0.3121	0.3128
0 wt.%	10000	0.3167	0.3144	0.3132	0.3142
Different (%)					
1 wt.%	2	0	0	0	0.0351
1 wt.%	6	0	0	0	0.0235
1 wt.%	10	0	0	0	0
1 wt.%	14	0	0	0.0227	0
1 wt.%	18	0	0	0.0226	0.0226
1 wt.%	10000	0	0	0	0.0225
0 wt.%	14	0	0	0	0
0 wt.%	10000	0	0	0	0

4.1.2 Effect of varying slenderness ratio L/h on dimensionless fundamental frequency increment (%) compared with $\Lambda_{GPL} = 0.0\%$ (porosity distribution 1, GPL pattern A, C–C copper-matrix beam, $e_0 = 0.5, n = 14$) is shown in Table 4.

Table 4 Result comparison on effect of varying L/h

Λ_{GPL}	$L/h = 20$	$L/h = 30$	$L/h = 40$	$L/h = 50$
Author's solution (Increment (%))				
0.0 wt.%	0.00	0.00	0.00	0.00
0.2 wt.%	9.58	9.65	9.67	9.69
0.4 wt.%	18.34	18.47	18.51	18.53
0.6 wt.%	26.44	26.63	26.69	26.72
0.8 wt.%	34.02	34.25	34.34	34.38
1.0 wt.%	41.16	41.44	41.54	41.59
Solutions done by Kitipornchai et al. (Increment (%))				
0.0 wt.%	0.00	0.00	0.00	0.00
0.2 wt.%	9.58	9.65	9.68	9.69
0.4 wt.%	18.34	18.47	18.52	18.54
0.6 wt.%	26.45	26.63	26.70	26.73
0.8 wt.%	34.03	34.26	34.35	34.39
1.0 wt.%	41.17	41.45	41.55	41.60
Different (%)				
0.0 wt.%	0	0	0	0
0.2 wt.%	0	0	0.1033	0
0.4 wt.%	0	0	0.0540	0.0539
0.6 wt.%	0.0378	0	0.0375	0.0374
0.8 wt.%	0.0294	0.0292	0.0291	0.0291
1.0 wt.%	0.0243	0.0241	0.0241	0.0240

4.1.3 Effect of different metal matrixes on dimensionless fundamental frequency increment (%) compared with $\Lambda_{GPL} = 0.0\%$ (porosity distribution 1, GPL pattern A, C–C beam, $L/h = 20, e_0 = 0.5, n = 14$) is shown in Fig. 4.

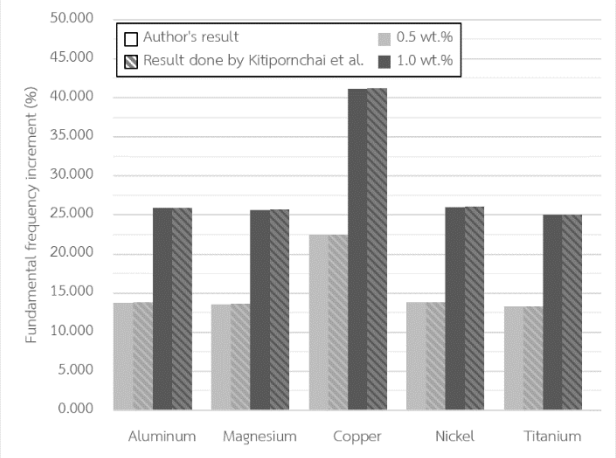

Fig. 4. Result comparison on effect of different metal matrixes.

4.1.4 Effect of GPL distribution pattern on dimensionless fundamental frequency (C–C copper-matrix beam, $L/h = 20, e_0 = 0.5, n = 14$) is shown in Fig. 5A, 5B and 5C.

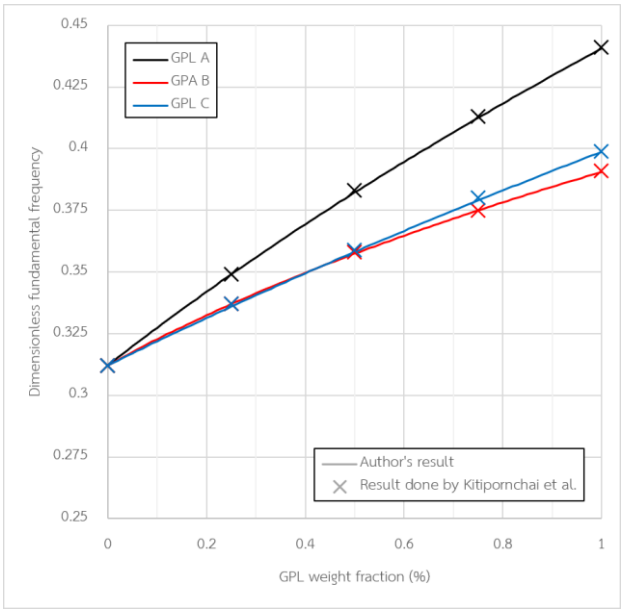

Fig. 5A. Result comparison on effect of different GPL distribution pattern (porosity distribution 1).

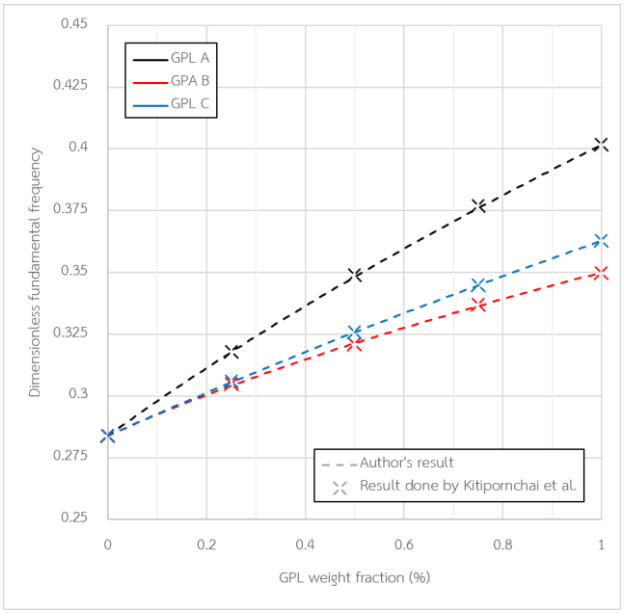

Fig. 5B. Result comparison on effect of different GPL distribution pattern (porosity distribution 2).

4.1.5 Effect of beam support types on dimensionless fundamental frequency increment (%) of various Λ_{GPL} compared with $\Lambda_{GPL} = 0.0\%$ (porosity distribution 1, copper-matrix beam, $L/h = 20$, $e_0 = 0.5$, $n = 14$) is shown in Fig. 6A, 6B and 6C

4.2 Convergence studies

Consider C–F copper beam with porosity distribution 2, GPL pattern B, $e_0 = 0.5$, $L/h = 20$, $\Lambda_{GPL} = 1.0\%$, $n = 10{,}000$.

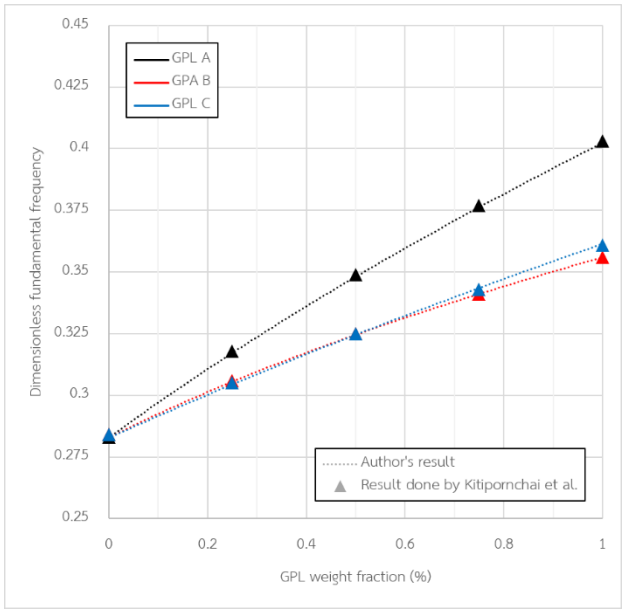

Fig. 5C. Result comparison on effect of different GPL distribution pattern (uniform porosity distribution).

Approximate solution done by using B-splines basis function with polynomial order $p = 2$ to 5 and varying number of basis functions n is shown in Table 5. where n, shown in Table 5, is the number of basis functions before the treatment of essential boundary conditions. So, the final size of the matrix system is $3n–3$.

The convergence study shows that using a higher order of basis functions, a smaller number of functions will be required to get the converged answer. As shown in Table 5, using $p = 2$, $n = 114$ will be required while using $p = 3$, $n = 22$ will be required, if considering the 6th decimal place.

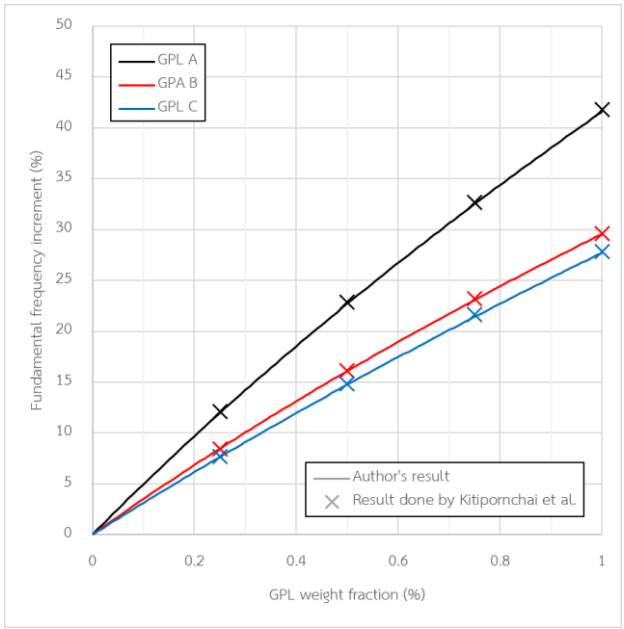

Fig. 6A. Result comparison on effect of different beam support types (H–H).

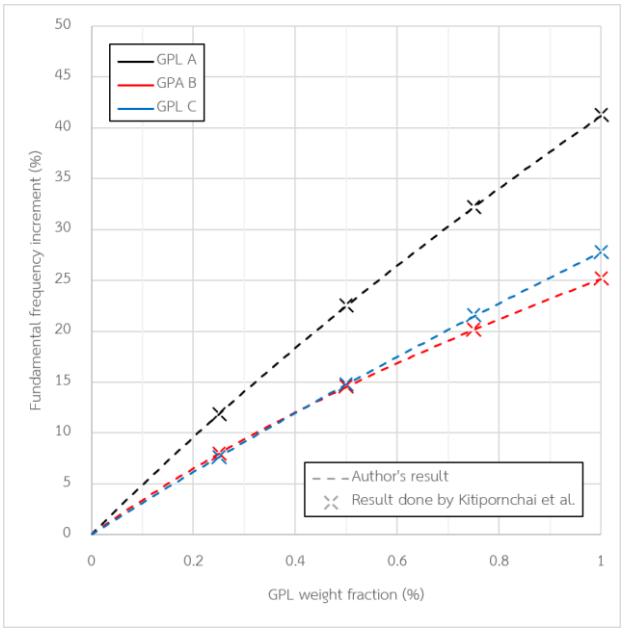

Fig. 6B. Result comparison on effect of different beam support types (C–C).

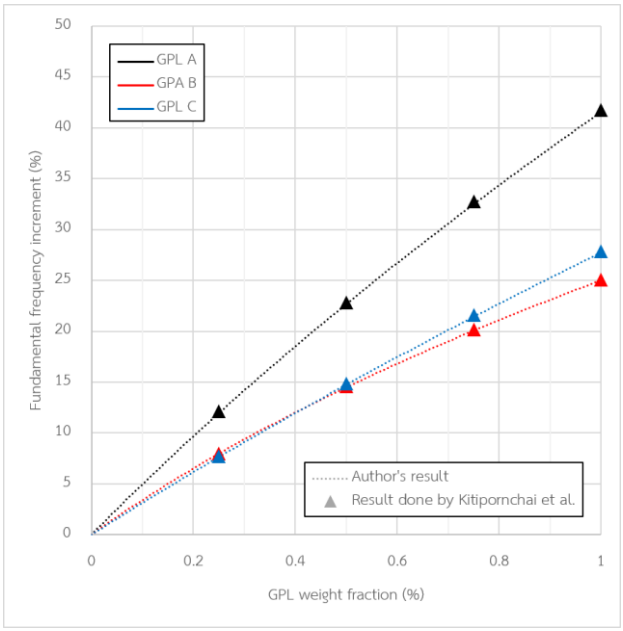

Fig. 6C. Result comparison on effect of different beam support types (C–F).

5. Conclusions

This project studies and develops a tool for calculating fundamental frequencies of functionally graded nanocomposite metal foam beams with GPLs dispersed using Isogeometric Analysis based on work done by Sritawat Kitipornchai, Da Chen and Jie Yang which used the Ritz method and uses their work as a reference answer.

The developed tool provides answers that converge to reference answers in terms of effect of varying porosity coefficients e_0 and number of layers n (as shown in Table 3),

Table 5 Approximate result from various polynomial order B-splines basis function.

n	$p = 2$	$p = 3$	$p = 4$	$p = 5$
1	–	–	–	–
2	–	–	–	–
3	1.844088	–	–	–
4	1.466594	1.283859	–	–
5	0.638366	0.407827	0.356598	–
6	0.445613	0.363422	0.356421	0.355571
7	0.390580	0.357220	0.355577	0.355405
8	0.371671	0.355808	0.355399	0.355373
9	0.363937	0.355489	0.355363	0.355355
10	0.360302	0.355402	0.355354	0.355353
11	0.358408	0.355374	0.355353	0.355352
12	0.357341	0.355363	0.355353	0.355352
13	0.356703	0.355358	0.355352	0.355352
14	0.356302	0.355355	0.355352	0.355352
15	0.356039	0.355354	0.355352	0.355352
16	0.355862	0.355353	0.355352	0.355352
17	0.355738	0.355353	0.355352	0.355352
18	0.355650	0.355353	0.355352	0.355352
19	0.355585	0.355353	0.355352	0.355352
20	0.355537	0.355353	0.355352	0.355352
21	0.355501	0.355353	0.355352	0.355352
22	0.355474	0.355352	0.355352	0.355352
23	0.355452	0.355352	0.355352	0.355352
24	0.355435	0.355352	0.355352	0.355352
25	0.355421	0.355352	0.355352	0.355352
26	0.355411	0.355352	0.355352	0.355352
27	0.355402	0.355352	0.355352	0.355352
28	0.355395	0.355352	0.355352	0.355352
29	0.355389	0.355352	0.355352	0.355352
30	0.355384	0.355352	0.355352	0.355352
31	0.355380	0.355352	0.355352	0.355352
32	0.355376	0.355352	0.355352	0.355352
⋮	⋮	⋮	⋮	⋮
112	0.355353	0.355352	0.355352	0.355352
113	0.355353	0.355352	0.355352	0.355352
114	0.355352	0.355352	0.355352	0.355352
115	0.355352	0.355352	0.355352	0.355352
116	0.355352	0.355352	0.355352	0.355352
117	0.355352	0.355352	0.355352	0.355352
118	0.355352	0.355352	0.355352	0.355352
119	0.355352	0.355352	0.355352	0.355352
120	0.355352	0.355352	0.355352	0.355352
121	0.355352	0.355352	0.355352	0.355352
122	0.355352	0.355352	0.355352	0.355352

effect of varying slenderness ratio L/h (as shown in Table 4), effect of different metal matrixes (as shown in Fig. 4), effect of GPL distribution pattern (as shown in Fig. 5A, 5B, 5C) and effect of different beam support types (as shown in Fig. 6A, 6B, 6C)

Then, the convergence study shows that using a higher order of basis functions, a smaller number of functions will be required to get the converged answer (as shown in Table 5).

In this project, Isogeometric Analysis and B-splines basis function have been applied only to the problem of 1D beams with uniform mapping. For future research, Isogeometric Analysis and B-splines basis function can be applied to more difficult shaped beams with more complex properties.

References

[1] L.-P. Lefebvre, J. Banhart, D. Dunand, Porous metals and metallic foams: current status and recent developments, Adv. Eng. Mater. 10 (2008) 775–787.

[2] B. Smith, S. Szyniszewski, J. Hajjar, B. Schafer, S. Arwade, Steel foam for structures: a review of applications, manufacturing and material properties, J. Constr. Steel Res. 71 (2012) 1–10.

[3] A. Hassani, A. Habibolahzadeh, H. Bafti, Production of graded aluminum foams via powder space holder technique, Mater. Des. 40 (2012) 510–515.

[4] S.-Y. He, Y. Zhang, G. Dai, J.-Q. Jiang, Preparation of density-graded aluminum foam, Mater. Sci. Eng. A 618 (2014) 496–499.

[5] Y. Hangai, K. Takahashi, T. Utsunomiya, S. Kitahara, O. Kuwazuru, N. Yoshikawa, Fabrication of functionally graded aluminum foam using aluminum alloy die castings by friction stir processing, Mater. Sci. Eng. A 534 (2012) 716–719.

[6] Y. Hangai, K. Saito, T. Utsunomiya, S. Kitahara, O. Kuwazuru, N. Yoshikawa, Compression properties of Al/Al–Si–Cu alloy functionally graded aluminum foam fabricated by friction stir processing route, Mater. Trans. 54 (2013) 405–408.

[7] N. Shafiei, A. Mousavi, M. Ghadiri, On size-dependent nonlinear vibration of porous and imperfect functionally graded tapered microbeams, Int. J. Eng. Sci. 106 (2016) 42–56.

[8] D. Chen, J. Yang, S. Kitipornchai, Free and forced vibrations of shear deformable functionally graded porous beams, Int. J. Mech. Sci. 108 (2016) 14–22.

[9] D. Chen, S. Kitipornchai, J. Yang, Nonlinear free vibration of shear deformable sandwich beam with a functionally graded porous core, Thin-Walled Struct. 107 (2016) 39–48.

[10] M.A. Rafiee, J. Rafiee, Z. Wang, H. Song, Z.-Z. Yu, N. Koratkar, Enhanced mechanical properties of nanocomposites at low graphene content, ACS Nano 3 (2009) 3884–3890.

[11] S. Kitipornchai, D. Chen, J. Yang, Free vibration and elastic buckling of functionally graded porous beams reinforced by graphene platelets, Materials & Design (2017) 656-665.

[12] A.P. Roberts, E.J. Garboczi, Elastic moduli of model random three-dimensional closed-cell cellular solids, Acta Mater. 49 (2001) 189–197.

[13] A. Roberts, E.J. Garboczi, Computation of the linear elastic properties of random porous materials with a wide variety of microstructure, Proceedings of the Royal Society of London A: Mathematical, Physical and Engineering Sciences, 2002.

[14] M. Shokrieh, M. Esmkhani, Z. Shokrieh, Z. Zhao, Stiffness prediction of graphene nanoplatelet/epoxy nanocomposites by a combined molecular dynamics–micromechanics method, Comput. Mater. Sci. 92 (2014) 444–450.

[15] J. Affdl, J. Kardos, The Halpin-Tsai equations: a review, Polym. Eng. Sci. 16 (1976) 344–352.

[16] R.G. De Villoria, A. Miravete, Mechanical model to evaluate the effect of the dispersion in nanocomposites, Acta Mater. 55 (2007) 3025–3031.

[17] F. Liu, P. Ming, J. Li, Ab initio calculation of ideal strength and phonon instability of graphene under tension, Phys. Rev. B 76 (2007) 064120.